Published in Supercond. Sci. Technol. 26 (2013) 045002

# Experimental and numerical analysis of quench propagation on $MgB_2$ tapes and pancake coils

J. Pelegrín[1], G. Romano[2], E. Martínez[1*], L.A. Angurel[1], R. Navarro[1], C. Ferdeghini[2], S. Brisigotti[3], G. Grasso[3] and D. Nardelli[3]

[1] *Instituto de Ciencia de Materiales de Aragón, (CSIC – Universidad de Zaragoza), Zaragoza, Spain*
[2] *CNR-SPIN, Genova, Italy*
[3] *Columbus Superconductors, Genova, Italy*

* Corresponding author: elenamar@unizar.es

**Keywords**: quench, thermal stability, $MgB_2$, 2D, superconductor, pancake coils

Classification numbers: 74.70.Ad, 74.25.F, 74.25.fc, 84.71.Mn

**Abstract**:

The study of the stability process of $MgB_2$ superconducting wires and coils is an important issue in the design and feasibility of electric power applications. In this sense, the thermal conductivity plays an important role, which in composite wires and tapes is mainly determined by the amount of stabilizer (usually copper), the configuration of filaments and the metallic matrix; while for coils, the winding, wire electric insulation and epoxy binder characteristics are added. In this paper we present results on quench development and propagation on isolated tapes, and small single pancake coils cooled by thermal conduction, for three types of $MgB_2$ tapes with different stabilization. The quench parameters; Minimum Quench Energy (*MQE*), Minimum Propagation Zone (*MPZ*), and normal zone propagation velocity ($v_p$) at different temperatures are reported.

A complete electrical and thermal characterization of the superconducting wires and of non-superconducting materials used in the coil manufacture has been made. With these data, numerical computational models using finite element simulations have been performed for isolated wires and single pancake coils and the results of the relevant quench parameters have been compared with the measured values.

This is an author-created, un-copyedited version of an article published in Superconducting Science and Techonology.
IOP Publishing Ltd is not responsible for any errors or omissions in this version of the manuscript or any version derived from it.

The Version of Record is available online at DOI: 10.1088/0953-2048/26/4/045002

## 1. Introduction

The analysis and characterization of the thermal stability of superconducting systems by local disturbances at working currents and temperatures is of great importance for the design and reliability of superconducting devices used in electric power applications, becoming crucial for those directly cooled by thermal conduction, *i.e.*; without heat exchange with cryogenic fluids.

Most thermal stability studies simulate the behaviour of superconducting systems during a quench fault (transition from the superconducting to the normal state), either by applying local heat pulses [1-6] or over-currents [7-11] and analyse the temperature and electric field profiles along the conductor wire and the system. These experiments allow the determination of the parameters that characterise the local appearance of a quench and its propagation to the overall conductor as: Minimum Quench Energy, *MQE*; normal zone propagation velocity or quench velocity, $v_p$; temperature profile around the disturbance, which gives the *M*inimum Propagation *Z*one, *MPZ*; quench current; etc.

Predictions given by Wilson's model [12] have been proven to be adequate to explain the quench behaviour of low temperature superconductors (LTS). Nevertheless, some aspects of $MgB_2$ and high temperature superconductors (HTS) performances differ from these predictions [3-6,13], due to some distinctive properties, such as the lower *n*-values of their current-voltage characteristics ($V \propto I^n$), which do not allow the use of critical state model approximations, and the wider differences between the operating and the critical temperatures, $T_0$ and $T_c$, respectively, which produce an extended current-sharing regime with the metallic matrix always present in real conductors.

To overcome these limits of Wilson's model in the analysis of quench behaviour on $MgB_2$ conductors and coils, one (1D), two (2D) and three (3D) dimensional numerical computational models have focused recent researches [3-5,14-16]. Nevertheless, most experimental results have been obtained on short straight conductor samples and 1D models were applied [3-5] in most cases, because their length dominates other dimensions, and further experiments on systems closer to real applications [17] and corresponding 2D and 3D simulations are welcome.

$MgB_2$ superconductors have been the subject of intense research since its discovery [18] and in the last years have been selected as a candidate for electric power

applications at operation temperatures about 20 K. Already long length metal/$MgB_2$ composite conductors with high critical currents values, $I_c$, fabricated by the Power-In-Tube (PIT) process, are commercially available. Most sheaths of composite $MgB_2$ conductors are Fe, Ni or alloys with low thermal conductivity and the use of a thermal stabilizer within the conductors is required. This is achieved introducing a metal with high thermal and electrical conductivities, usually Cu, which should not be in contact with $MgB_2$ to avoid chemical reactivity during heat treatments.

The increase of Cu amounts to improve wire's quench stability without decreasing the engineering critical current becomes an important technological issue. Here we report on the quench properties of three different $MgB_2$ composite tapes made with different dispositions and amounts of Cu. Heat pulse techniques to induce a quench and thermal conduction cooling are used in these measurements. Moreover, physically relevant quantities to the quench analysis of these tapes; self field critical current $I_c(T)$, electrical resistivity above $T_c$, $\rho(T)$, longitudinal thermal conductivity, $k(T)$, and heat capacity $c_p(T)$ as a function of the temperature, have been determined because of the importance of these parameters on the quench development.

Additional requirements should be fulfilled to reach quench stability in coils made with such $MgB_2$ conductors. Now to the tape's temperature dependences of the thermal and electric properties, it should be added the ones of impregnation materials needed to support the electromagnetic stresses during operation while keeping the electric insulation on neighbouring turns. To analyse these effects we report on the quench properties of three single pancake coils fabricated with these tapes and impregnated with epoxy. In the measurements, local heat pulse techniques with thermal conduction cooling were also used. Moreover, to guess on the radial thermal conductivity of the coils, $k_r(T)$, a stack of tapes with the same electric insulation and epoxy impregnation have been measured in the transverse direction.

Finally, the influence of the different wire's thermal stabilization and auxiliary coil winding materials on the quench parameters on tapes and coils has been analysed using numerical computational models in appropriated 1D and 3D geometries and boundary conditions.

## 2. Experimental

### 2.1 *$MgB_2$ conductors and characterization*

The three $MgB_2$ conductors analyzed in this study are multi-filament composite tapes fabricated by Columbus Superconductors using the PIT *ex-situ* technique. The differences of the three tapes used in this analysis can be observed in Figure 1 where back-scattered electron SEM images of polished cross-sections are collected.

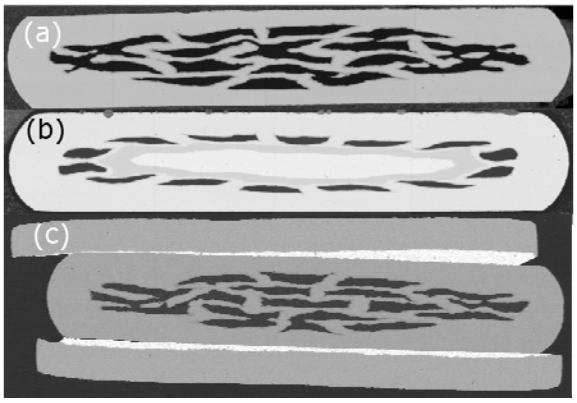


**Figure 1.** SEM micrographs of polished cross-sections of the analysed tapes: (a) tape A: 3.0×0.50 $mm^2$; (b) tape B: 3.6×0.65 $mm^2$ and (c) tape C: 3.0×0.9 $mm^2$. Explanations of the different contrasts of these pictures are given in the text.

Tape A has not thermal stabilizer. Its SEM image [Figure 1(a)] clearly shows nineteen $MgB_2$ superconducting filaments (black contrast inside), pure Ni sheaths (grey) which surrounds each filament and a thicker Ni (grey) outside sheath embracing all of them forming a Ni-$MgB_2$ composite with area (or volume) proportions about 80%-20%, respectively, and 3.0 mm × 0.50 mm cross-section.

The SEM image of tape B [Figure 1(b)] corresponds to the cross-section of a PIT standard Columbus commercial tape. It has fourteen Ni (lighter grey contrast) sheathed $MgB_2$ superconducting filaments (black contrast) placed around a Cu-core (white contrast), to facilitate the thermal stabilization of the conductor. A sheath of pure Fe (darker grey) surrounds the Cu-core to minimize its chemical reactivity with Ni during annealing. A thick Ni sheath (lighter grey) embraced the Cu/Fe core and the filaments. The resulting tape has 3.6 mm × 0.65 mm cross-section and the volume proportions of the elements are 67% Ni, 8% Fe, 15% Cu and 10% $MgB_2$.

Tape C is a sandwich of tape A after complete fabrication and two Cu sheets of 200 μm thickness and 3 mm width soldered at both tape sides. In the corresponding SEM micrograph of Figure 1(c), the Ni sheaths and the external Cu sheaths appears with the same grey contrast while the $MgB_2$ filaments are black and the soldering material (Sn-Pb alloy) white. The cross-section of tape C increases to 3.0 mm × 0.90

mm and the volumetric proportions of the composite elements are approximately 42% Ni, 42% Cu, 11% $MgB_2$ and 5% soldering *i.e.*; compared with tape B the amount of Cu increases by a factor 2.8 while keeping almost the same superconductor proportion.

The thermal and electric properties of these three tapes were fully characterized and the experimental results are showed in Figure 2.

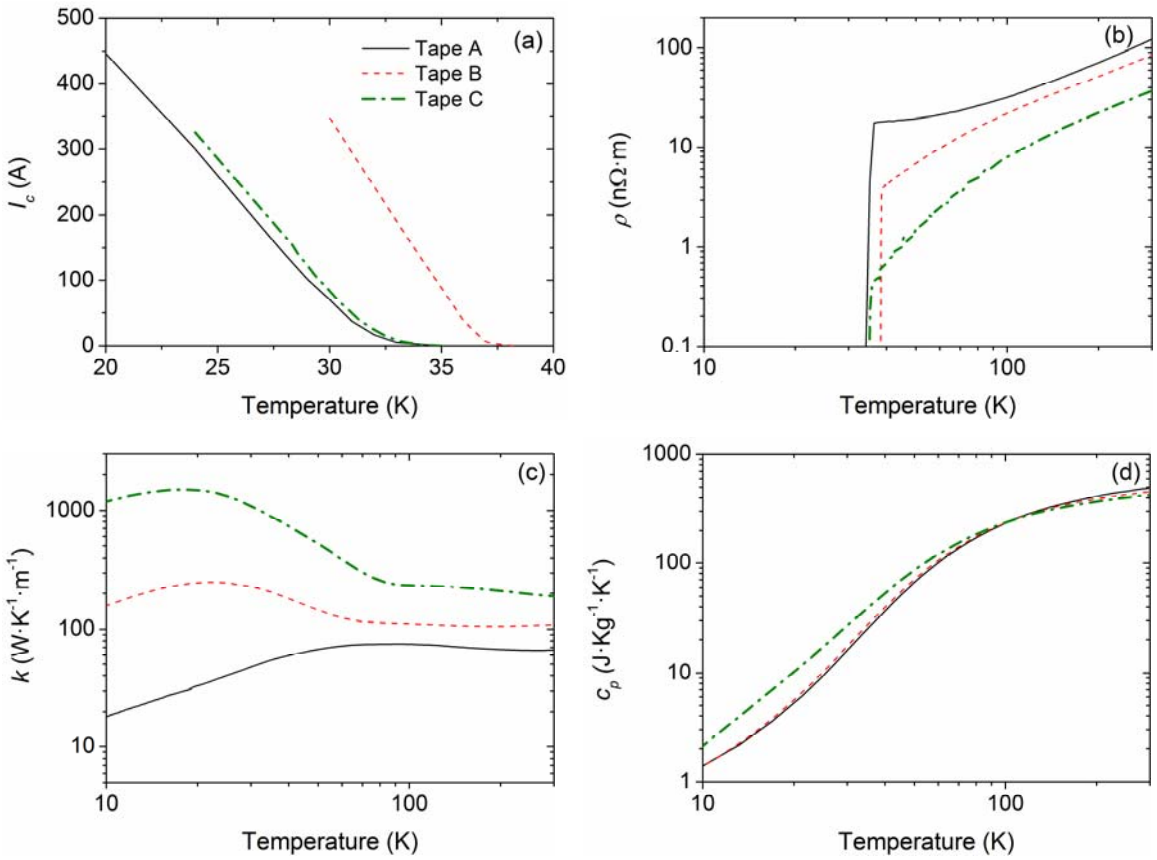


**Figure 2.** (a) Critical current, $I_c$; (b) electrical resistivity, $\rho$;, (c) thermal conductivity, $k$, and (d) heat capacity, $c_p$, as a function of the temperature for tapes A (continuous lines), B (dashed lines) and C (dot-dashed lines).

The self-field critical current, $I_c(T)$, was deduced from *I-V* measurements at different temperatures with the usual 1 μV/cm criterion. The exponent $n(T)$ values have also been derived by fitting this experimental data for $I>I_c$ to the relation $log(V) \propto n(T)log(I)$. The values of $n$ at 30 K are of the order of 30, 22 and 25 for tapes A, B and C, respectively, and decrease when the temperature approaches $T_c$. It must be noted that tapes A and C have the same critical temperature ($T_c$= 35 K) while for tape B it is slightly higher ($T_c$= 38 K) and $I_c(0)$ reaches higher values. The differences on $I_c(T)$ for tapes A and C are lower than 20%.

Electrical resistivity, $\rho(T)$, thermal conductivity along the tapes, $k(T)$, and heat capacity, $c_p(T)$, within 5% of accuracy, were measured at zero field using conventional methods in a Physical Property Measurement System (PPMS) from Quantum Design.

The $\rho(T)$ results above $T_c$ and $k(T)$ curves strongly change with temperature but also have wide relative differences due to the tape's Cu amounts; and logarithmic scales have been used in Figure 2 to allow the comparisons. Accordingly, the electrical resistivity values just above $T_c$ are 18, 4.0 and 0.5 nΩ·m for tapes A, B and C, respectively, due to the different Cu percentage. The $k(T)$ curves display broad maxima at 90 K, 22 K and 18 K for tapes A, B and C, respectively, and the corresponding values at 30 K; 50, 220 and 1100 $W \cdot K^{-1} \cdot m^{-1}$, clearly correlated with the amount of Cu.

On the contrary, as expected from the additive contribution of composite tape elements to the overall heat capacity, $c_p(T)$ follows analogous trends for the three tapes, being closed to the values obtained by the addition of corresponding ones of the separate components (with differences less than 8-10%). Tape C has higher $c_p(T)$ values than tapes A and B at low temperatures, which is due to the Sn-Pb soldering alloy, because in this range its $c_p(T)$ is almost one order of magnitude higher than those of the other metals present in the tapes.

### 2.2 *Coil fabrication and characterization*

One layer single pancake coils with heights given by the tape widths and inner and outer diameters, $Ø_{in}$=13 cm and $Ø_{out}$=16 cm, have been fabricated by hand winding. The inner diameter was fixed to be the minimum value required to avoid $I_c$ degradations during winding, while the dimensions of the cryostat limited $Ø_{out}$.

For easy measurements of voltage taps and thermocouples, thin and narrow (75 μm × 2.0 mm) 20 mm long copper sheets were soldered to the tape at given turns during coil winding as can be seen in the picture of Figure 3. In addition, feeding contacts made of Cu sheet (0.5 × 70 × 20 $mm^3$) were soldered at the coil ends.

The electric insulation between adjacent coil turns for tapes A and C was a fiberglass cloth tape 100 μm thick and 3 mm wide, while tape B was fully covered by a thin layer (50 μm) of electric insulator varnish (PEEK$^{TM}$) as provided by Columbus Inc. As tapes and insulation layers have different thicknesses, the winding has resulted in three coils with different number of turns; 20, 19 and 12 for tapes A, B and C, respectively (so far coils A, B and C).

During the measurements, the pancake coils are in vacuum and cooled only by thermal conduction. Thus, to insure a proper thermal contact, a 0.5 mm thick copper disk of diameter Ø≈ $Ø_{out}$, was attached to each pancake coil and thermally anchored to the 2nd stage of the cryocooler cold finger. To keep good thermal contact and electric insulation between the coil and the copper disc, a layer of Stycast 2850 FT epoxy (thickness about 250 μm) was hand painted in one of disc surfaces. After drying, the coil was placed onto the painted surface and the set impregnated with the same epoxy. Figure 3 (b) shows the Cu-disk/pancake-coil set once installed with all electric connections and anchored to the cryocooler cold finger.

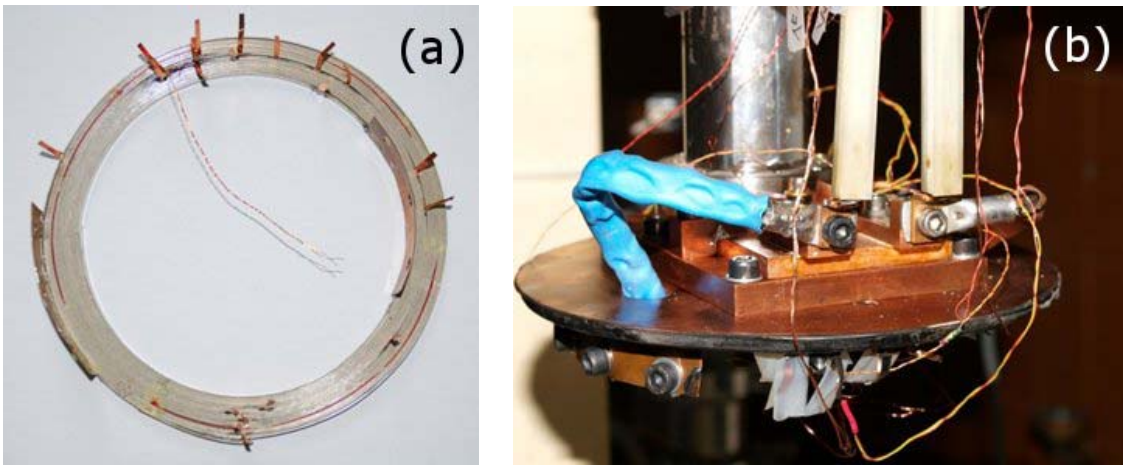


**Figure 3.** (a) Picture of one of the coils before epoxy impregnation showing voltage taps and current feeding contacts. (b) Cu-disc /coil set installed in the cold head of the cryocooler.

Previously to quench measurements, each Cu-disc/pancake-coil set was tested at low temperatures in order to ensure its homogeneity, verifying the absence of damages, electric short-circuits or $I_c$ performance degradation during winding and impregnation processes. With this aim, the $V(I)$ curves each 3-turns were recorded at several temperatures. The differences between the higher and the lower measured $I_c$ values in the different parts of a coil are in all cases lower than 10-12%.

For each tape type, a stack of 4 straight tapes electrically insulated as in the coils and impregnated with Stycast 2850FT epoxy has been used to estimate the effective radial thermal conductivity of the impregnated pancake coil, $k_r(T)$, by measuring in the tape's perpendicular direction using the above-mentioned PPMS. Moreover, similar conductivity measurements were done in small Stycast 2850 FT epoxy bars and the results are collected in Figure 4.

A comparison of these $k_r(T)$ results at 30 K gives values of 0.11, 0.08 and 0.15 $W \cdot K^{-1} \cdot m^{-1}$ for the stacks of tapes A, B and C, respectively, which are smaller than the

epoxy one $k$= 0.37 W·K$^{-1}$·m$^{-1}$. These differences only may be due to the poorer thermal conductivity of the electric insulation materials, being the lowest value for the stack made with tape B by its cover of PEEK varnish.

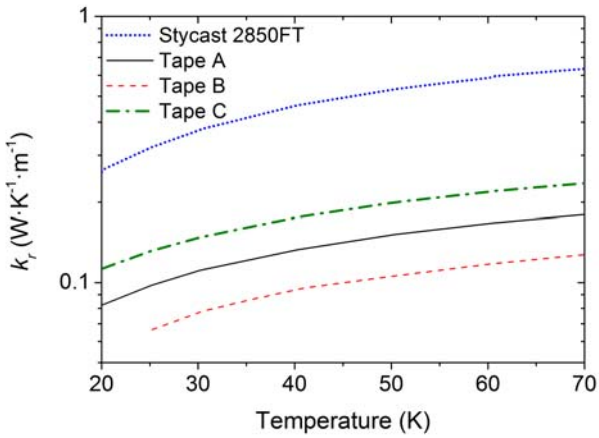


**Figure 4.** Temperature dependence of the thermal conductivity $k_r$ across stacks of electric insulated tapes impregnated by Stycast 2850FT for the three analyzed tapes. The $k(T)$ measurements of Stycast 2850FT bars are also shown.

2.3 *Experimental set-up for quench measurements*

In quench experiments, at given temperatures of the cryocooler cold finger, $T_0$, energy pulses, $Q_{ini}$, were deposited on isolated tapes or coils carrying different DC currents, $I<I_c(T_0)$ by passing through the heater rectangular current pulses of intensity $I_p$ and duration $t_p$. For that purpose a small strain gage 3 mm long, 2 mm wide and 0.4 mm thick, and 120 Ω of resistance was glued directly to the tape surface using GE varnish for the coils and Stycast epoxy for the tapes. The heater was always placed at equal distances of voltage taps $V_1$ and $V_2$. Additionally, $V_3$, $V_4$, $V_5$… were soldered to the conductor as shown in Figure 5, being the distance between them 5 or 10 mm, depending on the tape or coil. Thin copper wires, 0.1 mm of diameter, were soldered to the taps for isolated tape measurements, or to the copper sheets previously soldered to the winding, for coil experiments.

All the measurements were done in vacuum at different temperatures, recording the voltage of these taps simultaneously at different positions using a Data Acquisition (DAQ) device, being the maximum DC current of the experimental set-up limited to ≈ 150 A.

For tapes, the heater was positioned at the mid-distance of the feeding current contacts and the ends of the samples were anchored to the 2$^{nd}$ stage of the cryoocoler as explained in [3]. The length of the samples used in the measurements was $L$= 25 cm for

tapes B and C, while for tape A a shorter $L$= 10 cm was used to ensure a good thermalisation along the sample.

For the pancake-coil measurements, the heater together with the above mentioned distribution of voltage taps was placed in the mid-turn tape, but new taps $V'_1$, $V'_2$ and $V''_1$, $V''_2$ were also located at nearest and next-nearest outsider turns, respectively (see Figure 5).

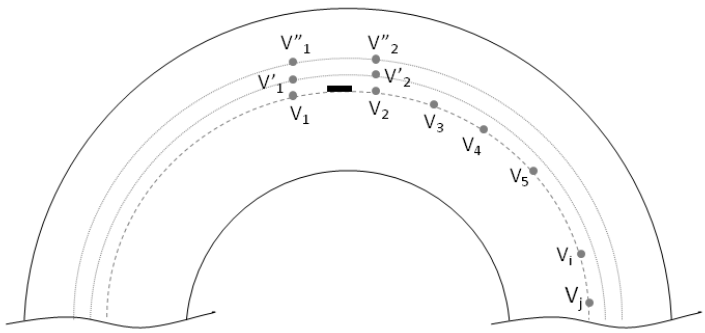


**Figure 5.** Schematic distribution of the voltage taps for the quench analysis on single pancake coils. The heater is placed in the mid-turn (dotted line) between voltage taps $V_1$ and $V_2$.

## 3. Numerical models

### *3.1. 1D numerical model for long tapes*

In 1D simulations, the heat balance equation with appropriated boundary conditions has been solved using an explicit finite differences method. For an arbitrary tape segment of length $\delta x$, this equation is reduced to:

$$d_0 c_p(T)\frac{\partial T}{\partial t} - \frac{\partial}{\partial x}\left(k(T)\frac{\partial T}{\partial x}\right) - G(T,I) - P_{ini}(x,t) = 0 \qquad (1)$$

Here the coordinate $x$ gives the segment position (centre) along the tape, $t$ is the time and $d_0$ the average mass density of the wire. Three time and space functions are also involved in equation (1): $T(x,t)$, distribution and evolution of local tape temperatures; $P_{ini}(x,t)$, input heater power pulse density, which for $0<t<t_p$ and at the heater length, $L_h$, is constant, $Q_{ini}/(L_h \cdot A \cdot t_p)$, and zero elsewhere, being $A$ the tape cross-section and $Q_{ini}$ the overall energy of the heat pulse; and $G(T,I)$, the average Joule power dissipation per unit volume due to the tape's superconductor and composite metals sharing currents, which is given by $G(T,I)= I \cdot E(T,I)/A$, being $I$ the transport current and $E(T,I)$ the local electric field.

In equation (1), the experimental temperature dependences measured for the longitudinal thermal conductivity and heat capacity of the tapes were used. Moreover, the current sharing temperature, $T_s$, and the Joule heating powers $G(T,I)$ were calculated for each tape using the experimental $\rho(T)$, $I_c(T)$ and $E\sim [I/I_c(T)]^{n(T)}$ functions. Firstly, $T_s$ was determined for each intensity $I$, from the relation $I_c(T_s)= I$. Afterwards, it has been assumed that $G(T,I)$ is zero for temperatures below $T_s$, while for the current sharing regime ($T_s(I)\leq T\leq T_c$) the conductor can be modelled as two parallel electric impedances: one ohmic through the metal matrix with a resistivity obtained by smooth extrapolation of experimental $\rho(T)$ above $T_c$ to temperatures below, and another associated to the power-law voltage-current relation of the superconductor.

In all simulations, long enough tapes were used to ensure that the quench generation and propagation is not affected by finite size effects, *i.e.*, effectively it would be equivalent to use adiabatic boundary conditions. Furthermore, the thermal resistance between the tapes and the heater has been neglected.

*3.2. 3D numerical models for Cu-disc/pancake-coil sets*

The constructed sets of cooper disc and impregnated single pancake coils have been modelled as a stack of four elements: the copper disc, the epoxy layer used to join the Cu disc and the coil keeping good thermal contact and electric insulation between them, the heterogeneous coil (tapes, electric insulation and epoxy impregnation) and the epoxy layer that covers the winding after the impregnation (see Figure 6). The experimental data of $I_c(T)$, $\rho(T)$, $k(T)$ and $c_p(T)$ here reported for tapes and stack of tapes, completed with required ones of Cu and the $c_p(T)$ of Stycast 2850FT, taken from literature [19], were used to fix the physical properties of the involved elements in each 3D model.

Two different numerical finite element approaches [15] have been used to solve the 3D heat diffusion equation:

$$\nabla \cdot (k\nabla T) + P(\mathbf{r},T) + P_{ini}(\mathbf{r},T) = d_0 c_p(T)\frac{\partial T}{\partial t} \qquad (2)$$

**i)** *Continuum medium models (CM)* [see Figure 6(a)]. The impregnated coil is approached by an anisotropic effective medium with thermal conductivities $k_t$ and $k_r$ along the tangential (azimuthal) and radial directions, respectively. $k_t$ is approximated by the thermal conductivities measured on isolated tapes and $k_r$ by the ones of epoxy impregnated stack of tapes. In a small region of the Cu-disc/pancake-coil set [dark gray

contrast in Figure 6(a)] the power density due to the heater, $P_{ini}(\mathbf{r},T)$ is $Q_{ini}/(L_h \cdot A_h \cdot t_p)$ during the heat pulse, $0<t<t_p$, and zero elsewhere; where $L_h$= 3 mm (as the length of the used strain gage), $A_h = w_t \cdot (e_t/5)$ (being $w_t$ and $e_t$ the width and the thickness of the tape, respectively). Moreover, the Joule heating power density $P(\mathbf{r},T) = f_{sc} \cdot G(T,I)$ extends along the winding area, being $f_{sc}$ the filling factor of the superconducting tapes in the winding.

**ii)** *Full 3D (FULL3D) models* [Figure 6(b)]. They follow the heterogeneous distribution of superconducting tapes and electric insulation layers within the pancake coil, which includes the fibreglass or varnish and the epoxy impregnation and uses the specific tape's electric and thermal properties. Now, the power heater density $P_{ini}(\mathbf{r},T) = Q_{ini}/(L_h \cdot A_h \cdot t_p)$ takes place only within the tape in a small region of the coil, while the Joule heating density $P(\mathbf{r},T) = G(T,I)$ is restricted to the tape.

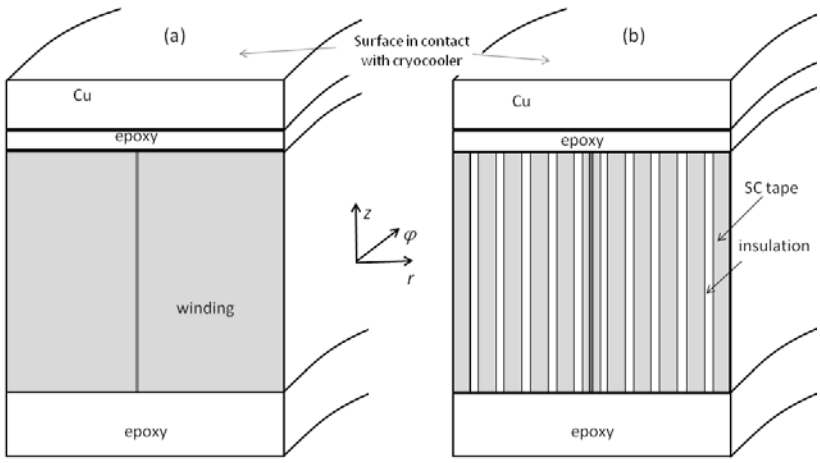


**Figure 6.** Scheme (not to scale) of the Cu-disc/pancake-coil cross-section at the heater position used in quench development and propagation simulations in (a) CM and (b) FULL3D models. Darker grey area in the center of the winding corresponds to the region where the heat pulse ($Q_{ini}$) is introduced.

FULL3D models also require data of transverse thermal conductivities of the tapes, which are estimated from their microstructure and the measured longitudinal components, and of the electric insulation layers between adjacent tape windings.

For example, the thermal conductivity of tape A has been estimated from its microstructure to be similar in the azimuthal and *z*-directions of the coil ($k_{t,\varphi} = k_{t,z} = k$) but smaller in the radial direction $k_{t,r} \approx k/3$, being $k(T)$ the measured longitudinal component This *k*-anisotropy is similar to the observed ones in Bi-2223 tapes [20], which share a comparable disposition of flat superconducting parallel filaments separated by metallic sheaths.

The effective thermal conductivity of the insulating layers between adjacent turns in the winding, $k_{in}$, which is assumed to be isotropic, may be estimated considering a series association of tapes and insulating layers thermal resistances:

$$\frac{e_t+e_{in}}{k_r} = \frac{e_t}{k_{t,r}} + \frac{e_{in}}{k_{in}}, \quad (3)$$

where $e_{in}$ is the insulation layer thickness and $k_r(T)$ the transverse conductivity measured on the stacks of tapes. As for all tapes, $e_t/k_{t,r} << e_{in}/k_{in}$, equation (3) relates directly $k_{in}$ with $k_r$.

It must be remarked that the tape's thermal conductivity anisotropy has minor relevance in the experimental values and the numerical simulations of the coil's radial properties because the thermal conductivity of the impregnated electric insulation are much smaller. Then, the anisotropy of the thermal conductivity of the pancake coils is mainly due to the low $k$ value of the insulating layers.

In both 3D models, the real spiral path of the tape within the pancake coil is neglected. This approach is valid if the tangential heat diffusion along the whole turn takes much longer than that of radial heat diffusion into the adjacent turn, *i.e.* when $\tau_t/\tau_r >>1$, where the time constants in the tangential and radial directions, $\tau_t$ and $\tau_r$, respectively, can be estimated by [21]:

$$\tau_t = (\pi \emptyset_{in})^2 \frac{c_p}{k_t} \quad \text{and} \quad \tau_r = (e_t + e_{in})^2 \frac{c_p}{k_r} \quad (4)$$

It has been observed from the simulations that this condition is fulfilled for coils A and B, but not for coil C.

In most cases, CM numerical modelling of coils have been followed, since it requires less number of grid elements, and therefore much less computational memory and time than the FULL3D model. The latter have been used to simulate coil A in order to compare the results with those of CM. In addition, two different boundary conditions have been considered:

i) Constant temperature boundary conditions *i.e.*; assuming that the surface of the copper disc in contact to the cryocooler cold finger does not heat up during a quench, keeping constant the temperature $T_0$.

ii) Thermal insulation of the Cu-disc/pancake coil, *i.e.*, assuming that the system has not heat interchange with the surroundings during the quench (adiabatic condition).

## 4. Results and discussion

*4.1. Long straight tapes (1D case)*

*Minimum quench Energy (MQE)*

The *MQE* values obtained experimentally using heat pulses of duration $t_p$= 200 ms, energies up to 300 mJ and different reduced intensities $I/I_c$ have been collected in Figure 7 together with 1D numerical estimates. The temperatures have been chosen to have the same $I_c$ values in all tapes. In particular, the results corresponding to $I_c$= 100 A and $I_c$= 140 A are presented. For $I_c$= 100 A, the operation temperatures are $T_0$= 29 K, 34.5 K and 29.4 K for tapes A, B and C, respectively; while for $I_c$= 140 A, these values are $T_0$= 28 K and 33.7 K for tapes A and B, respectively.

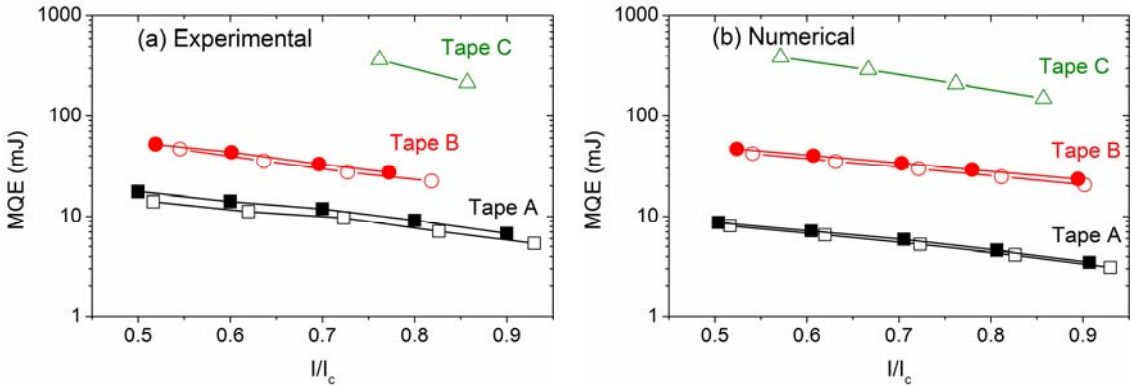


**Figure 7.** Experimental and numerically simulated *MQE* values as a function of the reduced current $I/I_c$ for tapes A –squares, tape B –circles and tape C –triangles. Open symbols are used for $I_c$= 100 A and closed ones for $I_c$= 140 A, corresponding to the temperatures given in the text.

For the analysed temperatures and currents the experimental *MQE* values are between 5 to 20 mJ for tape A, from 20 to 50 mJ for tape B and around 300 mJ for tape C. *MQE* becomes notably higher when the amount of Cu increases from 0% to 15% and to 42%. The agreement of these results with the corresponding numerical simulations is good for tapes B and C, obtaining differences below 10%, while for tape A the experimental results are ≈ 80% higher.

In order to analyse the reasons of these discrepancies in *MQE*, we have considered into the 1D model the heater's thermal conductivity and heat capacity contributions to the tape quench using its real dimensions and the amount of epoxy used to fix it. With this improvement, the differences between *MQE* results and estimations for tapes B and C become less than 5% (*i.e.*; within the errors of the used input data) but for tape A the numerical estimations are still ≈20% lower. Further consideration of the solder contribution to the numerical simulations, gives differences within 5% of the experimental ones. These results point-out the relevance of the heater,

sticking epoxy, wire contacts and solder contributions to *MQE*, which becomes maximum on tape A.

The larger relative distortions introduced by the needed experimental addenda onto the tape A measurements compared with tapes B and C ones are explained by their different *MPZ* values. Identifying *MPZ* as the length of the sample above the sharing temperature, *i.e.*; the tape length with electric field above a given value when the quench is triggered, the experimental recording of the electric fields along the tape enable to determine *MPZ* [3,5]. For tape A, the *MPZ*'s obtained both experimentally and numerically are smaller than 1 cm; for tape B they range between 1.5 cm and 4.5 cm; while for tape C, they are longer than the tape samples length, 25 cm, for all considered current and temperature conditions. From 1D simulations a value *MPZ*= 1.2 m has been estimated for tape C. Therefore, samples longer than 2 m would be necessary in this case, which cannot be managed in our experimental set-up.

Therefore, for tape A, which has a very short *MPZ* (< 1 cm), the internal energy changes and the involved heat flow contributions, compare with the ones of the 3 mm long heater, sticking epoxy and solder, giving the larger discrepancies between experimental and numerical *MQE* values. However, for tapes B and C, the *MPZ* lengths are one or two orders of magnitude longer, and the relative contributions to the thermal energy storage and conduction of all addenda needed to perform the measurements become less important. It should be remarked that similar conclusions have been reported analysing the quench on coated conductors [22].

*Quench propagation velocity* ($v_p$)

The experimental results and the numerical estimations of the quench propagation velocity $v_p$ of tapes A and B have been represented in Figure 8, for the same $I_c$ and $T_0$ values used in Figure 7. As previously advanced, it was not possible to measure $v_p$ in tape C because the sample's length was shorter than the *MPZ* one.

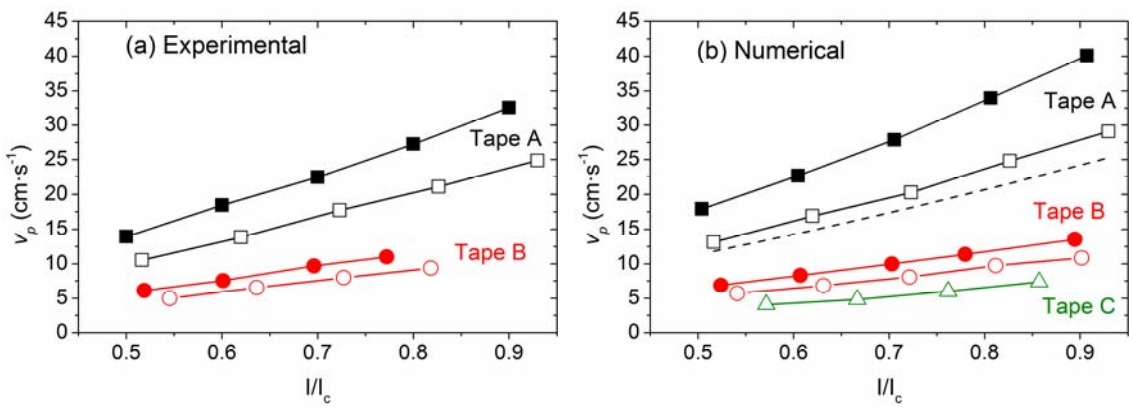

**Figure 8.** Experimental and numerically estimated values of the quench propagation velocity $v_p$ as a function of the reduced current, $I/I_c$, for tapes A –squares, B –circles and C –triangles. Open and full symbols correspond to $I_c$ of 100 A and 140 A, respectively. Wilson's quench prediction for tape A and $I_c$ = 100 A (dashed line) is also included.

As usual, the experimental quench propagation velocity $v_p$ for a given reduced current $i= I/I_c$ is faster for lower temperatures because of the higher $I_c(T)$ and the lower $c_p(T)$ values. In addition, the $v_p(T)$ values for tape A are about 2.2 times faster than for tape B, ratio which qualitatively conforms Wilsons´s quench model predictions [12]:

$$v_p = \frac{I}{Ad_0 c_p}\left(\frac{\rho k}{T_m - T_o}\right)^{1/2} \tag{5}$$

where $T_0$ is the operation temperature and $T_m>T_0$ the mid-value between the sharing and the critical temperature, $T_m=(T_s+T_c)/2$.

The comparison of the $v_p$ experimental results with corresponding 1D numerical estimations are somewhat higher than the experimental ones, 20% for tape A and 10 % for tape B. This difference is reduced to less than 5% taking into account the additional mass of the wires used to measure the voltage along the tape. Its presence is equivalent to an increase of the effective heat capacity, which will reduce the propagation velocity, in agreement with previous reports on YBCO tapes [22]. On the other hand, Figure 8(b) also shows similar $v_p$ values for tapes B and C, indicating that the different amount of stabilizer is determinant for the quench generation but not for its propagation.

The differences of the $v_p$ estimations obtained with Wilsons´s quench model [12] and those from 1D simulations are less than 10% as shown in Figure 8 for tape A and $I_c$= 100 A. Similar agreements have been obtained for the other tapes and currents but by search of clarity, they have not been represented in the Figure.

*4.2. Pancake coil case*

Figure 9 shows characteristic records of the time evolution of average electric fields between the adjacent voltage taps shown in Figure 5 for tape and coil A with $I$= 90 $A$ ($i$= 0.9), using heat pulses of 200 ms with energies of 5.4 mJ and 28 mJ, respectively, and starting in both cases at $t$= 0. $E_{ij}$ is the voltage measured between taps $V_i$ and $V_j$ divided by the distance between them.

The measurements of the voltage appearance within the mid turn taps allow the determination of the tangential quench propagation velocities, while the ones of adjacent turns, give the radial direction components. It is observed that the velocities along the tapes in the pancake coils are slower than in tapes.

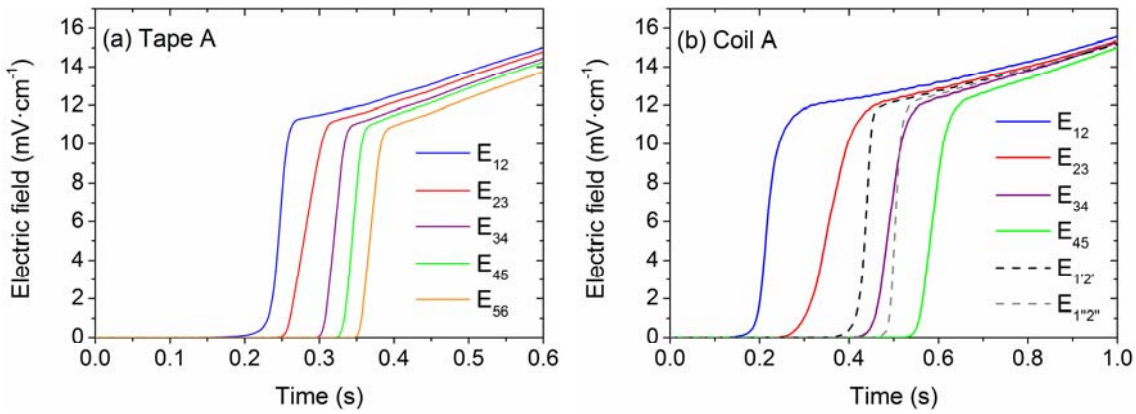


**Figure 9.** Time evolution of average electric fields observed amid voltages taps during a quench at $I$=90 A, $I_c$=100 A, for (a) tape A at $T$= 29 K; and (b) pancake coil A at $T$= 28 K. In (b) continuous and dashed lines correspond to electric fields along the mid-turn tape and between the taps placed in adjacent turns, respectively (see Figure 5). Taps distances in the straight tape were 10 mm for $E_{12}$ and $E_{23}$, and 5 mm for the rest; while in the coil were 10 mm.

*Minimum quench Energy (MQE)*

The experimental *MQE* values and the numerical estimations derived with the CM model as a function of the reduced current are shown in Figure 10. The measurements were performed at temperatures such that $I_c$= 100 A (28 K for coil A, 33 K for coil B and 29 K for coil C) and $I_c$= 150 A (26 K for coil A and 30 K for coil B). Note the use of smaller temperatures for coils because the magnetic self-field decreases $I_c$. The length of the heat pulses was $t_p$= 200 ms for coil A. Although for quench comparison it would be preferable the use of short heat pulses of the same duration $t_p$ for all coils, the maximum attainable heater power during 200 ms was not enough to produce the quench in coils B and C. For this reason, heat pulses between 600 and 1500 ms were used for coil B and between 3700 and 5000 ms for coil C.

The experimental *MQE* are between 20 and 50 mJ for the pancake coil A, between 450 and 1000 mJ for coil B and between 6000 and 8000 mJ for coil C.

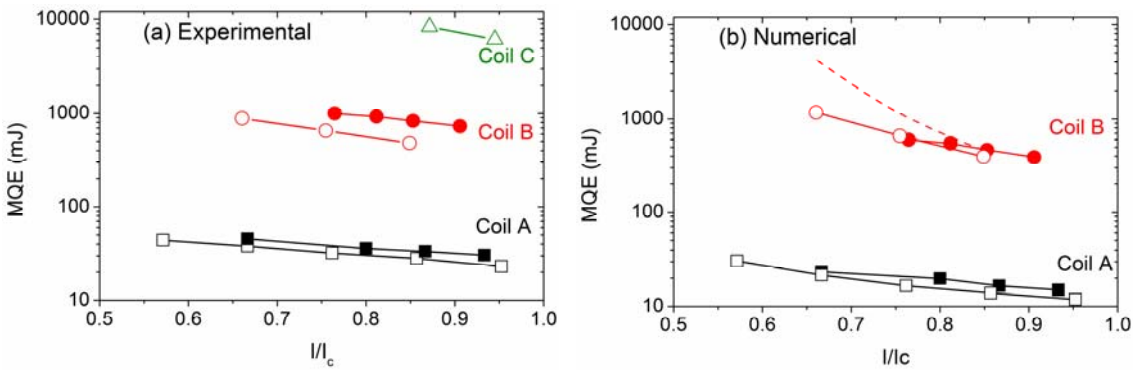


**Figure 10.** Experimental and numerical *MQE* results as a function of the reduced current for coils A – squares, B –circles and C –triangles. Open symbols correspond to $I_c$= 100 A while closed ones to $I_c$ = 150 A (the coil temperatures are given in the text). The numerical estimates correspond to adiabatic boundary conditions in all cases, except for the discontinuous line, which corresponds to isothermal condition of the Cu surface of coil B and $I_c$= 100 A.

For coil A, the *MQE* values estimated with the CM model for both isothermal and adiabatic boundary conditions have differences lower than 2%, but are almost half the experimental ones. Moreover, the FULL3D model estimations are about 20% higher than those of the CM model, which do not gap the differences. For example, at $T_0$= 28 K and $I/I_c$= 0.85, *MQE* values of 14 mJ, 17 mJ and 28 mJ have been obtained by CM, FULL3D and experimentally, respectively. As for tape A, the contributions of the addenda used in the experiments may explain these differences.

For coil B, the CM simulations using adiabatic boundary conditions gives *MQE* values 40% lower than the corresponding experimental results for $T_0$= 30 K ($I_c$=150 A), while for $T_0$= 33 K ($I_c$=100 A) the differences are below 20%. It should be reminded that $t_p$ values between 600 to 1000 ms, used experimentally and in the simulations, are too long for the adiabatic approach. This may be the origin of the significant differences among the experimental *MQE* values and the simulations. On the other hand, considering constant operation temperatures, $T_0$, for the external Cu disk surface during the quench, the *MQE* simulations are, as expected, considerably higher than for adiabatic conditions. Depending on $T_0$ and reduced currents, the differences range from 20% to more than 300% for lower reduced currents and higher operation temperatures, as it can be seen in Figure 10(b). These results suggest that neither isothermal nor adiabatic assumptions describe the experimental results for this coil. Heat flow transfer from the winding to the cryocooler will occur during the quench enough slow to break the effective thermal insulation and of sufficient amount to change the temperature of the copper disc surface. Nevertheless, adiabatic conditions give better qualitative agreement with experimental *MQE* results.

For coil C, the CM simulations using adiabatic boundary conditions gives *MQE* values of the same order but lower than the corresponding experimental ones. The same considerations than for coil B would also apply to this coil. Moreover, for this coil the used model is not strictly valid, since the spiral path of the tapes should be taken into account, as discussed in 3.2.

*Quench propagation velocity ($v_p$)*

The experimental and numerical $v_p$ values, in tangential and radial directions, are shown in Figure 11, at $T_0$= 28 K for coil A and $T_0$= 33 K for coil B ($I_c$= 100 A in both cases). Due to the longer length of the *MPZ* in coil C (more than 8 turns) it was not possible to measure $v_p$ for this coil.

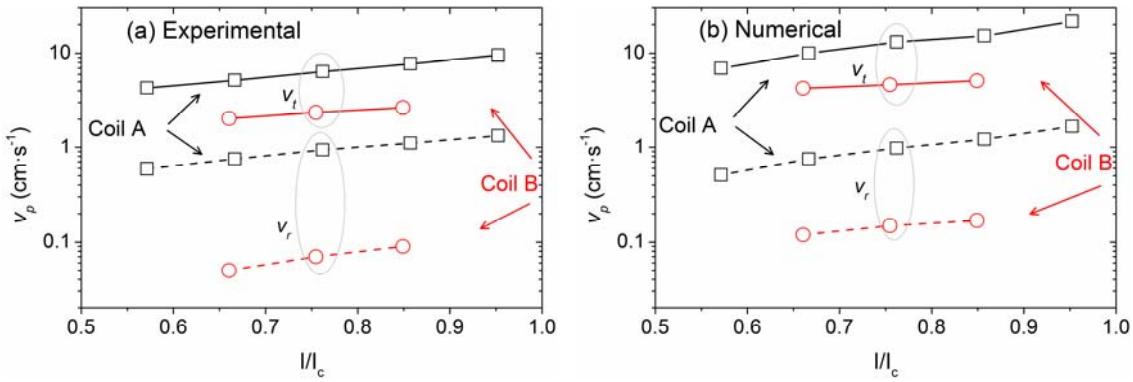


**Figure 11.** Experimental and CM numerical $v_p$ values, as a function of the reduced current, with $I_c$ = 100 A: squares for coil A ($T_0$= 28 K) and circles for coil B ($T_0$= 33 K). Continuous and dashed lines are used for tangential and radial $v_p$ components, respectively. CM estimates are for adiabatic boundaries.

In Figure 11(a) it is remarkable the low experimental values of the radial velocity component of coil B, which are associated to the lowest $k_r$ of the electric insulation varnish layer. In addition, there are large changes of the $v_p$ anisotropy (ratio of tangential versus radial components $\eta$=$v_t/v_r$), which is $\eta$≈7 for coil A and becomes $\eta$ ≈30 for coil B. It must be noted that the tape's propagation velocities are almost three times the tangential $v_p$ measured on the pancake coils, which is a trend already reported from numerical simulations of coils [14,15].

For coil A, the CM estimated tangential velocities are nearby twice the experimental ones, while for the radial velocities the agreement is very good (within the 10%). The $v_p$ values obtained by FULL3D models for adiabatic conditions are about 25% higher than those obtained by CM ones, *i.e.*; they are closer to the experimental values. For example, at 28 K and $I/I_c$= 0.85, longitudinal $v_p$ values of 16 cm/s, 13.5 cm/s and 7.5 cm/s have been obtained, respectively, by CM and FULL3D estimations and experimentally. Moreover, the differences of the propagation velocities for adiabatic and isothermal boundary conditions in this coil are about 10%. The smaller experimental values of the longitudinal $v_p$ may be due to the contribution of the amount of solder used to attach the Cu sheets to the tape's turns, which would increase the thermal inertia giving larger effective $c_p$ and consequently longitudinal $v_p$ values lower than those of taps free coils. When this contribution is taken into account, simulated longitudinal $v_p$ values decreases about a 15-20%.

For coil B, CM estimations for adiabatic conditions give tangential and radial propagation $v_p$ values twice the experimental ones. Nevertheless, considering constant temperature of the Cu-disc during the quench lowers $v_p$ values considerably, becoming even smaller than the experimental ones at higher $T_0$ and lower reduced currents. Since it has much lower propagation velocities than coil A, the heat transfer to the cryocooler

during the quench would not be negligible, explaining the lower experimental propagation velocities compared to the adiabatic CM estimations.

## 5. Conclusions

The quench behaviour of $MgB_2$ composite tapes with three different amounts of Cu (0%, 15% and 42%) as thermal stabilizer on samples cooled by thermal conduction has been measured with local heat pulse methods for different temperatures and currents. Two order of magnitude changes in the characteristic quench parameters have been found being correlated with the Cu content: *MPZ* values ranging from less than 1 cm to more than 100 cm and *MQE* values from minimum values of about 10 mJ to 400 mJ, respectively, for tapes of 0% and 42% of Cu.

The *MQZ*, *MQE* and $v_p$ results for straight tapes have been analysed with finite elements numerical models in one dimension, using the experimental $I_c(T)$, $\rho(T)$, $k(T)$ and $c_p(T)$ data also reported for these tapes. Good agreement, within the accuracy of the experimental data used-5%, has been found between the experimental *MPZ* and *MQE* results and the theoretical estimates when the heater and voltage taps contributions are taken into account, being of major importance in tapes without thermal stabilizer. Similar quality experimental –theoretical agreement has been obtained for $v_p$ but also does not show differences with Wilsons's quench model formulas.

The quench behaviour of single pancake coils made with these composite tapes cooled by thermal conduction and derived by the short heat pulses method has also been reported. The *MQE* experimental values for the single pancake coils are about one order of magnitude higher than corresponding ones for straight tapes; while the longitudinal propagation velocities are lowered by a factor of three.

CM or FULL3D numerical simulations for adiabatic boundary conditions show the same reduced current trends than the experimental values, although with differences in the absolute values. For coils made with low thermal conductivity tapes, these differences have been attributed to the larger relative contribution of the addenda needed to perform the quench measurements. The shortness of the *MPZ*, gives relevance to the heater, Cu taps and solder (whether using tin or indium alloys) contributions, due to the increase of the thermal inertia giving larger effective $c_p$.

For coils made with tapes of high thermal conductivity, as longer heat pulses has been used, the main origin of the differences between adiabatic simulations and

experiments would be due to the heat flow transfer to the cryocooler that would be enough to break the effective thermal insulation and to change the temperature of the copper disc surface. Nevertheless, adiabatic conditions during the quench give better qualitative agreements with experimental *MQE* results than considering constant temperatures of the Cu disc used to thermalize the coil.

**Acknowledgments**

Funding of this research by Spanish MINECO and the European FEDER Program (Project MAT2011-22719) and by Gobierno de Aragón (Research group T12) is gratefully acknowledged. J.P. acknowledges financial support from the Spanish Ministry of Education, Culture and Sports, (FPI program). C.F. wishes to thank the PRIN 20082BBZ9W for the financial support.

## References


[1] Wang X, Trociewitz U P and Schwartz J 2007 *J. Appl. Phys.* **101** 053904

[2] Ishiyama A, Yanai M, Morisaki T, Ueda H, Shiohara Y, Izumi T, Iijima Y and Saitoh T, 2005 *IEEE Trans. Appl. Supercond.* **15** 1659

[3] Martínez E, Young E A, Bianchetti M, Muñoz O, Schlachter S I, Yang Y 2008 *Supercond. Sci. Technol.* **21** 025009 (8pp)

[4] van Weeren H, van den Eijnden N C, Wessel W A J, et al. 2005 *IEEE Trans. Appl. Supercond.* **15** 1667

[5] Martínez E, Muñoz O, Angurel LA, Yang Y and Schlachter S I, 2009 *IEEE Trans. Appl. Supercond.* **19** 3533

[6] Young E A, Friend C M, Yang Y 2009 *IEEE Trans. Appl. Supercond.* **19** 2500

[7] Kwon N Y, Kim H S, Kim K L, Yim S W, Kim H-R, Hyun O-B, Kim H M and Lee H G, 2009 *Supercond. Sci. Technol.* **22** 045003

[8] Furuse M, Yamasaki H, Manabe T, Sohma M, Kondo W, Yamaguchi I, Kumagai T, Kaiho K, Arai K and Nakagawa M, 2007 *IEEE Trans. Appl. Supercond.* **17** 3479

[9] Kim H M, Jankowski J, Lee H, Bascuñán J, Fleshler S and Iwasa Y, 2004 *IEEE Trans. Appl. Supercond.* **14** 1290

[10] Peroz C, Villard C, Buzon D and Tixador P 2003 *Supercond. Sci. Technol.* **16** 54

[11] Martínez E, Angurel L A, Pelegrín J, Xie Y Y and Selvamanickam V 2010 *Supercond. Sci. Technol*. **23** 025011

[12] Wilson M N, "Superconducting Magnets" 1983 (Oxford: Clarendon)

[13] Huang T, Martínez E, Friend C and Yang Y, 2008 *IEEE Trans. Appl. Supercond.* **18** 1317

[14] Stenvall A, Mikkonnen R, Kovac, 2010 Physica C **470** 2047

[15] Alessandrini M, Majkic G, Laskaris ET and Salama K, 2009 *IEEE Trans. Appl. Supercond.* **19** 2437

[16] Majkic G, Alessandrini M, Laskaris ET and Salama K, 2009 *Supercond. Sci. Technol.* **22** 034021

[17] Cavalieri V, Matrone A, Masullo G, Quarantiello R, Saggese a, Pace S. Gambardella U, 2008 *IEEE Trans. Appl. Supercond.* **18** 924

[18] Nagamatsu J, Nakagawa N, Murakanaka T, Zenitani Y and Akimitsu J 2001 *Nature* **410** 63

[19] Ekin JW "Experimental techniques for low-temperature measurements", Oxford University Press.

[20] Lehtonen J, Mikkonnen R and Paasi J, 2000 *Cryogenics* **40** 245

[21] Huang T, Ph D thesis, University of Southampton, (2006)

[22] Pelegrín J, Martínez E, Angurel LA, Xie Y-Y and Selvamanickam V, 2011 *IEEE Trans. Appl. Supercond.* **21** 3041